ChemPhysMater 1 (2022) 203–210

Contents lists available at ScienceDirect

ChemPhysMater

journal homepage: https://www.keaipublishing.com/en/journals/chemphysmater/

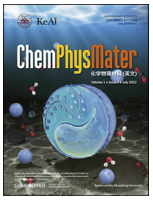

Research Article

Brain-targeted polymersome codelivery of siRNA and temozolomide for effective glioblastoma chemo-RNAi synergistic therapy

Meng Zheng[a,b,#], Chengnan Yan[a,b,#], Qingshan Yang[a,b], Feiyan Zhu[a,b], Qiuli Du[a,b], Xue Xia[a,b], Marco Morsch[c], Albert Lee[c], Jinglong Yin[a,b], Yan Zou[a,b,c], Bingyang Shi[c,*]

[a] Henan-Macquarie University Joint Centre for Biomedical Innovation, School of Life Sciences, Henan University, Kaifeng 475004, China
[b] Henan Key Laboratory of Brain Targeted Bio-nanomedicine, School of Life Sciences and School of Pharmacy, Henan University, Kaifeng 475004, China
[c] Department of Biomedical Sciences, Faculty of Medicine, Health and Human Sciences, Macquarie University, Sydney, Australia

ARTICLE INFO

Keywords:
Polymersome
siRNA
TMZ
Glioblastoma
Brain targeting

ABSTRACT

Temozolomide (TMZ) is a clinically approved drug for glioblastoma (GBM) therapy. However, as a result of methylguanine-DNA-methyltransferase (MGMT), which is able to repair damaged DNA-damage repairing, TMZ usually yields unsatisfactory therapeutic effects. Small interfering RNA (siRNA) is a potential alteration tool for sensitivity of TMZ by targeting DNA repair enzymes. However, a suitable TMZ and siRNA codelivery system that can effectively and actively co-deliver siRNA/TMZ into the brain tumor is lacking. In this study, we constructed an angiopep-2 decorated polymersomal delivery system to co-deliver TMZ/siRNA for synergistic GBM therapy. This targeted polymersomal nanomedicine not only enhanced the circulation time of siRNA/TMZ in blood but also improved their blood-brain barrier (BBB) crossing and GBM targeting ability. Moreover, when we co-administered siRNAs specific to retinoblastoma binding protein 4 (RBBP4) together with TMZ in GBM cells, these RBBP4-specific siRNA (siRBBP4) modulated the sensitivity of TMZ by regulating MGMT, and thus showed a powerful synergistic anti-tumor effect. We demonstrated that angiopep-2 decorated polymersomal siRBBP4/TMZ co-loaded nanomedicines are capable of inhibiting tumor growth and significantly improved life expectancy of orthotropic GBM bearing mice. Overall, our study suggests that such a polymersomal TMZ/siRNA codelivery system provides a robust and potent nanoplatform for targeted GBM chemo-RNAi therapy.

1. Introduction

The most prevalent type of malignant tumor in the central nervous system is glioblastoma (GBM) [1,2]. The GBM prognosis remains dismal, with a median survival of 15 months and a 5-year survival rate of fewer than 3% [3]. GBM is routinely treated with temozolomide (TMZ) chemotherapy in conjunction with surgery and radiation[4]. TMZ, as a DNA-alkylating agent, results in DNA damage and, subsequently, cell death in GBM cells [5].

Unfortunately, TMZ chemotherapy generally yields unsatisfactory therapeutic effects due to loss of sensitivity in glioma cells [6]. The mechanism underlying the development of TMZ insensitivity is not well established. The best described mechanism involves DNA repairing mediates by O^6-methylguanine DNA methyltransferase (MGMT) enzyme [7–9]. Some GBM patients with low-level expressed MGMT are more responsive to TMZ-based therapy [10]. However, even in tumors with low MGMT expression, other pathways have been shown to independently modulate responses to therapy and patient outcomes [11]. For example, retinoblastoma binding protein 4 (RBBP4) was identified as a TMZ sensitivity modulator that regulates MGMT expression [12]. Therefore, the combination of RBBP4 modulation with TMZ treatment is a promising avenue for enhancing TMZ sensitivity in glioma cells and conceivably expands the life expectancy of GBM patients. Among the applicable approaches, such as gene expression modulation, RNA interference (RNAi) has long been attractive because of its specificity and high efficacy [13–15]. In fact, small interfering RNA (siRNA) employed to specifically target and subsequently block or downregulate drug-resistance-related genes has been widely used to reverse chemical drug sensitivity [16]. For instance, p-glycoprotein (P-gp), epidermal growth factor receptor (EGFR), and myeloid cell leukemia sequence-1 (Mcl-1) specific siRNAs have been used to increase the sensitivity of doxorubicin (Dox) [17], erlotinib [18], and paclitaxel (PTX) [19], respectively. Thus, based on the merits of successes in siRNA/drug combination applications, regulation of RBBP4 expression by its targeting siRNA combined with TMZ is considered a desirable design for GBM treatment by increasing the sensitivity of TMZ. Nevertheless, the distinct chemical characteristics

* Corresponding author.
E-mail address: bingyang.shi@mq.edu.au (B. Shi).
# Both the authors contributed equally to this work.

https://doi.org/10.1016/j.chphma.2022.01.001
Received 23 August 2021; Received in revised form 16 December 2021; Accepted 1 January 2022
Available online 9 February 2022

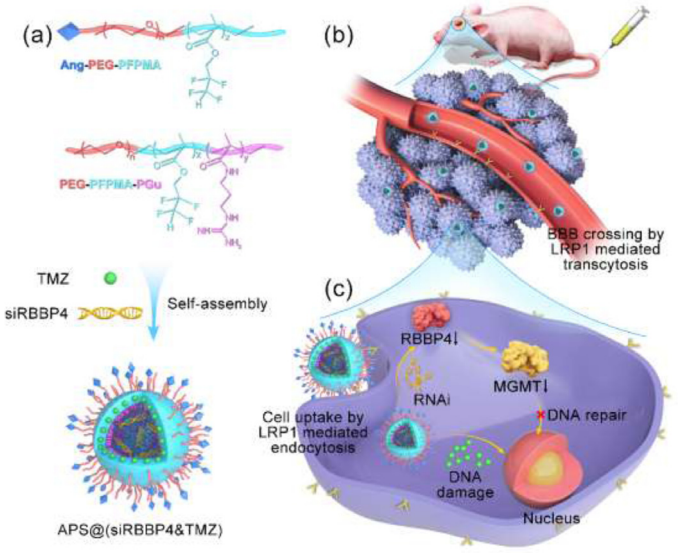

Fig. 1. Schematic illustration of APS@(siRNA&TMZ) for chemo-RNAi combinational glioblastoma (GBM) therapy. (a) Ang-PEG-PFPMA and PEG-PFPMA-PGu polymer mixture can self-assemble into polymersomes, which can be loaded with TMZ and siRNA. The formulated nanomedicine is denoted as APS@(siRNA&TMZ). (b) APS@(siRNA&TMZ) can efficiently cross the BBB and actively target GBM through Angiopep-2 ligand-mediated BBB transcytosis and GBM cell endocytosis. (c) After uptake into GBM cells, the delivered siRNAs can knockdown the RBBP4, leading to the downregulation of MGMT (which can repair the TMZ-damaged DNA) and the resulting enhancement of the sensitivity of TMZ in glioma cells.

(e.g., solubility, size, and charge) of TMZ and siRNA have impeded the design of nanocarriers encapsulating both drugs. Furthermore, the existence of the blood-brain barrier (BBB) reduces the efficacy of most therapeutic entities including nanomedicines [20–22]. Therefore, a suitable drug delivery system that can effectively co-deliver siRNA and TMZ and while also being carried across the BBB and accumulating in the brain tumor is undoubtedly preferable.

Polymer nanoparticles (such as micelles [23], polymersomes [24], nanogels [25], dendrimers [26], polymer-lipids [27,28]) have great potential for drug delivery for diverse disease treatments owing to their desirable biocompatibility, capacity for large-scale production, and ease of flexible modification [29]. Polymersome is an excellent drug delivery system because of its capacity to load a wide range of drugs with diverse chemical properties [30–32]. Polymersome nanostructures have aqueous interiors and hydrophobic walls, enabling them to contain both hydrophilic and hydrophobic specimens. This drug-loading versatility endows polymersomes as one of the most promising delivery platforms, particularly in combinational therapies, where encapsulation of multiple drugs with various chemical properties is highly advantageous.

In this study, we developed an Angiopep-2 decorated chimeric polymersome to co-deliver TMZ and siRNA (APS@(TMZ&siRNA)) for synergistic therapy of GBM (Fig. 1). This polymersomal nanoparticle was fabricated by self-assembly of Angiopep-2 decorated poly-(ethylene glycol)-block-poly-(2,2,3,3-tetrafluoropropyl methacrylate) (Ang-PEG-b-PFPMA) diblock polymers and poly-(ethylene glycol)-block-poly-(2,2,3,3-tetrafluoropropyl methacrylate)-block-poly[(N-(3-methacrylamidopropyl) guanidinium) (PEG-b-PFPMA-b-PGu) triblock polymers. Notably, the fluorinated hydrophobic median layer is expected to stabilize the self-assembled polymeric nanoparticles as well as encapsulate TMZ [33–35], while the positively charged guanidinated polymer chains self-assemble in the aqueous interiors and are capable of encapsulating the negatively charged siRNAs [36–38]. This polymersome was capable of actively targeting GBMs in the brain because of its Angiopep-2 mediated BBB crossing capacity and GBM targeting ability. Angiopep-2 peptide is readily interacts with the lipoprotein receptor–related protein-1 (LRP-1) receptor, which is overexpressed on the surface of endothelial cells of BBB as well as GBM cells [39–43]. Our studies showed that TMZ/siRNA co-loaded polymersomal nanomedicine (APS@(TMZ&siRNA)) exhibited prolonged blood-stream circulation, ideal BBB infiltration, outstanding tumor intensification and retention, potent in vitro and in vivo synergistic anti-tumor impacts, and effective inhibition of tumor progression, as well as a substantial improvement in the median survival time of orthotopic GBM bearing nude mice.

2. Materials and methods

2.1. Materials

2,2'-Azobis-(2-methylpropionitrile) (AIBN) and 2,2,3,3-tetrafluoropropyl methacrylate (FPMA) were obtained from J&K. Angiopep-2 peptide terminated with a thiol group and temozolomide (TMZ) were purchased from China Peptides Co., Ltd. and Sigma-Aldrich, respectively. N-(3-methacrylamidopropyl) guanidinium chloride (Gu), methoxy-poly(ethylene glycol)-4-cyanopentanoic acid dithionaphthalenoate (MeO-PEG-CPADN, 2 kDa PEG), and maleimide-poly(ethylene glycol)-CPADN (Mal-PEG-CPADN, 3.4 kDa PEG) were synthesized as previously reported [33]. The siRNAs used were purchased from GenePharma Company having the following sequences: (1) scramble: 5'-UUCUCCGAACGUGUCACGUdTdT-3' (sense); 5'-ACGUG ACACGUUCGGAGAAdTdT-3' (antisense); (2) siRBBP4: 5'-GCUGAA GUGAACUGCCUUUTT-3' (sense); and 5'-AAAGGCAGUUCACUUCA GCTT-3' (antisense). The 5′-terminal of the antisense strand of scrambled siRNA was labeled with Cy5.

2.2. Characterization

The polymers' ^{1}H-NMR spectra were detected using an AVANCE III spectrometer (HD 400 MHz, Bruker, Switzerland). At 25 °C, the particle size of the generated nanoparticles was determined using dynamic light scattering (DLS, Zetasizer Nano-ZS, Malvern Instruments) with a 633 nm He-Ne laser and backscattering detection. For confocal laser scanning microscopy (CLSM), a Zeiss 880 confocal microscope equipment was used to take the photographs. Transmission electron microscopy (TEM) photographs were collected for morphological characterization exploiting a JEM-2100 TEM (JEOL, Japan) at a 200 kV accelerating voltage. A multi-modal microplate reader (Molecular Devices, USA) was exploited to examine cellular transfection, and flow cytometry was used to quantify fluorescence (FACS (BD) Calibur, San Jose, CA, USA). Gel electrophoresis micrographs were captured using a Molecular Imager FX instrument (Bio-Rad, Hercules, CA, USA).

2.3. Synthesis of PEG-b-PFPMA

MeO-PEG-CPADN (40 mg, 20 μmol), FPMA (145 mg, 725 μmol), and AIBN (0.5 mg, 3 μmol) were dissolved in dried DMSO and sealed in a flask under the nitrogen protection. The reaction was carried out at 70 °C for 48 h. Then, the reaction mixture was cooled down to 25 °C and dialyzed versus DMSO continuously for 2 days and finally with water for additional 1 day. After freeze-drying, a yield of 69.2% was obtained from the final product of 128 mg PEG-b-PFPMA. The number of FPMA units in PEG-b-PFPMA was 24, as determined by ^{1}H NMR spectroscopy.

2.4. Synthesis of PEG-b-PFPMA-b-PGu

PEG-b-PFPMA (70 mg, 10 μmol), Gu (20 mg, 109 μmol), and AIBN (0.25 mg, 15 μmol) were again dissolved in dried DMSO and sealed in a flask under the protection of nitrogen, and proceeded to react at 70 °C

for 48 h, followed by cooling down to 25 °C and dialyzed against water for 2 days. The final product of PEG-b-PFPMA-b-PGu (75 mg, yield: 83.3%) was obtained by freeze-drying. Gu units in PEG-b-PFPMA-b-PGu was 4.5, as determined by ^{1}H NMR spectroscopy.

2.5. Synthesis of Ang-PEG-b-PFPMA

Angiopep-2 (50 mg, 20.8 μmol) and Mal-PEG-CPADN (50 mg, 14.7 μmol) were dissolved in DMSO and oxygen was removed by vacuum followed by stirring overnight at 37 °C. The solution was dialyzed with 3.4 kDa MWCO dialysis bag versus DMSO for 2 days and then water for additional 1 day. The product Ang-PEG-CPADN (61 mg, yield: 51.3%) was obtained by freeze-drying. The conjugation ratio of Angiopep-2 was 92.5%, as determined by the BCA assay. The synthesis of Ang-PEG-b-PFPMA was identical to that of PEG-b-PFPMA, as described above. The number of FPMA units in Ang-PEG-b-PFPMA was 23.5, as determined by ^{1}H NMR.

2.6. Preparation of polymersomal nanomedicine

siRNA and/or TMZ-loaded polymeric nanomedicine were prepared via the solvent exchange method. Typically, 50 μL of DMSO solution of PEG-b-PFPMA-b-PGu (20 mg/mL) was incubated with a prescribed amount of siRNA (10 mg/mL) in HEPES buffer (10 mM) at pH 7.4 and/or TMZ in DMSO (20 mg/mL). Afterward, the mixture was supplemented to 900 μL of HEPES buffer. The resulting dispersion was rested overnight at room temperature, and subsequently dialyzed (Spectra/Pore, MWCO 14000) versus HEPES buffer for 12 h. The angiopep-2 peptide decorated polymersomal nanomedicine (APS) was prepared using an Ang-PEG-b-PFPMA and PEG-b-PFPMA-b-PGu mixture at a molar ratio of 1:4. The size, distribution, and nanostructure morphology of the obtained polymersomal nanomedicines were measured using DLS and TEM, respectively. The amount of TMZ in the aqueous phase was checked at 327 nm using a multimodal microplate reader (Molecular Devices). For TMZ (%) estimation in the nanomedicine, their drug loading content (DLC) and drug loading efficiency (DLE) was determined by the formula described below:

$$DLC = \frac{m_1}{m_1 + m} \times 100\%,$$

$$DLE = \frac{m_1}{m_0} \times 100\%,$$

where m_1 is the mass of the loaded drug, m is the mass of the polymer, and m_0 is the mass of the feeding TMZ.

2.7. Gel retardation assay

Agarose gel was prepared using agarose in TEA buffer at a concentration of 1 wt.%. The agarose powder was dissolved by heating and allowed to cool before the addition of gel red (1 μL). The wt.% of siRNA to PEG-b-PFPMA-b-PGu was set at 10, 20, 30, and 40 wt.%. For gel electrophoresis, the siRNA-encapsulated nanomedicine was loaded into the gel and run at 30 V for 30 min in TEA running buffer. Following that, gel pictures were taken using the Molecular Imager-FX (Bio-Rad) at the excitation/emission wavelengths of 532/605 nm and examined using Quantity One software program (Bio-Rad).

2.8. MTT assay

To begin, a population of 1×10^4 U87MG or U251MG cells/well were grown in 96-well plates for 24 h. After removing the culture media, it was replaced with fresh medium (100 μL) holding empty polymersomes. After 48 h, the culture media was changed with new medium (100 mL) supplemented with 10% of a 5-mg/mL 3-(4,5-dimethylthiazol-2-yl)-2,5-diphenyltetrazoliumbromide (MTT) solution. At the end of 4 h further incubation and subsequent culture medium removal, then the live cells generated formazan was dissolved in 150 μL DMSO, and the absorbance (570 nm) of individual wells were detected through a multi-modal microplate reader. The cell viability measurements are presented as the mean deviation of 4 repeats.

2.9. In vitro trans-endothelial migration via trans-well BBB model

To determine the permeability of Angiopep-2 decorated polymersomes across the BBB, the in vitro BBB model was constructed using a monolayer of immortalized mouse brain endothelial bEnd.3 cells (5×10^4 cells/trans-well) placed on the top chamber of culture inserts (Corning, NY, USA). The trans-wells were then placed into 24-well plates, where the lower chamber kept filled with DMEM medium (800 μL) and refreshed every 2 days. After the bEnd.3 monolayer trans-endothelial electrical resistance (TEER) value reached higher than 200 Ω cm^2, then the upper chamber cell DMEM medium was exchanged with 190 μL serum-free DMEM, and 10 μL PS@Cy5-siRNA or APS@Cy5-siRNA was supplemented to reach the final siRNA concentration of 200 nM. The transwells were allowed to shake on a shaker (37 °C, 50 r/min). At 2, 4, 6, 8, and 12 h, aliquots (200 μL) were collected from the lower compartment and replaced with the equivalent volume of fresh medium. To confirm the retained monolayer integrity of the bEnd.3 cells, TEER value was determined again to check at the termination of the test. Finally, the percent transport ratio of siRNA nanomedicine was measured from the fluorescence of the collected samples using a multimodal microplate reader under the excitation/emission of 630 nm and 670 nm.

2.10. Cell uptake of polymersomal nanomedicine

Flow cytometry assay: U87MG and U251MG carcinomas were cultivated in a 6-well plate at a cellular intensity of 1×10^6 cells per well in Dulbecco's modified Eagle's media added with 10% FBS and then incubated with APS@Cy5-siRNA, PS@Cy5-siRNA, or Cy5-siRNA alone (siRNA concentration, 200 nM) at 37 °C. After incubation for 4 h, the treated cells were detached using 0.25 wt.% percent trypsin and 0.03 wt.% EDTA, followed by 3 min of centrifugation at 1000 r/min. The precipitated cell lines were rinsed with phosphate-buffer saline (PBS) for 2×3 min before being resuspended in PBS (500 μL) and examined directly using a flow cytometer (BD FACS Calibur) and Cell Quest software.

Confocal microscopy imaging: 1×10^5 U87MG or U251MG cells per well cultured on microscopic plates were incubated with APS@Cy5-siRNA, PS@Cy5-siRNA, or naked Cy5-siRNA (200 nM siRNA) at 37 °C for 4 h followed by subsequent medium removal and washing in PBS for 3×3 min. After 15 min of fixation with 4% paraformaldehyde (PFA), the samples were cleaned three times with PBS. The nuclei were marked with Hoechst (10 g/mL) and then rinsed in PBS before being photographed with a Zeiss 880 confocal laser scanning microscope.

2.11. Western blot analysis

The 24-well plates seeded U87MG and U251MG cells were grown overnight in DMEM medium. Carcinomas were then co-incubated with PBS, PS@(siRBBP4&TMZ), APS@(siScr&TMZ), APS@(siRBBP4&TMZ), or APS@siRBBP4 for 4h and in fresh DMEM culture media with 10% FBS for a further 48 h. The doses of siRNA and TMZ used were 200 nM and 20 μg/mL, respectively. Before being lysed with RIPA buffer, the treated cells were rinsed 2x with cold PBS. A 10% SDS-PAGE gel was used to separate the cell lysates, which were then transported to nitrocellulose membranes. Then, the proteins were immunoblotted with primary antibodies (MGMT, RBBP4, and β-actin from Servicebio, Wuhan, China) for 12 h at 4 °C. The immunoreactive protein bands visualization was performed by using peroxidase-labeled secondary antibodies (Servicebio) and the Amersham Imager 680 system (GE).

2.12. γH2AX DNA damage foci analysis by immunofluorescence

On poly-L-lysine coated glass coverslips, U87MG and U251MG cells were grown. Cells were treated with PBS, PS@(siRBBP4&TMZ), APS@(siScr&TMZ), APS@(siRBBP4&TMZ), or APS@siRBBP4 for 4 h. The incubation growth media was then replaced with new complete culture media and cultivated for another 48 h. The cell growth media was again removed, and the cell lines were rinsed 3x with PBS before being fixed with 4% PFA (20 min). The fixed cells were then blocked with goat serum for 1 h before being treated with γH2AX antibody (EMD Millipore) at 1/1000 dilution for 1 night at 4 °C. Subsequently, another 3x PBS washing was performed and then incubated with secondary antibody (Alexa Fluor, Invitrogen,), and Hoechst (1/1000 dilution) for 1 h at ambient temperature. A Zeiss 880 confocal microscope was used to image the coverslips mounted glass slides on ProLong Gold Antifade Mountant (Thermo Fisher).

2.13. Pharmacokinetics study

All animal handling protocols and experiments in this study were approved by the Medical and Scientific Research Ethics Committee of Henan University School of Medicine (China) (HUSOM-2020-176). All protocols of the animal studies conformed to the Guide for the Care and Use of Laboratory Animals. All animals in this study are female. The treatment groups include the APS@Cy5-siRNA, PS@Cy5-siRNA, or naked Cy5-siRNA were injected via tail vein into nude mice ($n = 3$) at an equivalent dosage of siRNA (1 mg/kg) in HEPES (200 μL). At the desired time-points post-injection, approximately 50 μL of blood was collected from the eye sockets. Next, the collected blood specimens were centrifuged immediately (15 kr/min, 30 min), and the level of Cy5 was measured in the supernatant as a function of fluorescence intensity using a microplate reader under excitation of 630 nm and emission of 670 nm. By Origin software 2018b, the exponential decay 2 model was used to calculate the half-lives by fitting the experimental data as follows: $y = A_1 \times \exp(-x/t_1) + A_2 \times \exp(-x/t_2) + y_0$, and then taking $t_{1/2}$, $\beta = 0.693 \times t_2$.

2.14. In vivo imaging visualization

To test the in vivo tumor-targeting potential, APS@Cy5-siRNA, PS@Cy5-siRNA, or Cy5-siRNA alone (siRNA, 1 mg/kg) were injected (i.v) into orthotopic U87MG-Luc glioma-implanted nude mice and then tracked at pre-determined time points exploiting a Lumina IVIS-III imaging system with excitation at 620 nm and emission at 670 nm.

2.15. Biodistribution in orthotopic U87MG-Luc glioma-implanted nude mice

APS@Cy5-siRNA, PS@Cy5-siRNA, or Cy5-siRNA alone (siRNA, 1 mg/kg) were administered into orthotopic U87MG-Luc glioma implanted nude mice through tail vein at 15 days post-implantation. The tumor-bearing animals were euthanized 4 h after the injection. The primary organs (heart, liver, spleen, lung, kidney, brain and tumor) were taken, cleaned, and weighed. The IVIS Lumina III system was used to capture ex vivo fluorescence photographs of the main organs. To determine the quantity of Cy5-siRNA, the organs were homogenized in 1 percent Triton X-100 (0.6 mL) using a homogenizer (JXFSTPRP-48). The supernatant was obtained after centrifugation of the organ samples at 15 kr/min for 30 min, and the Cy5-siRNA was quantified using a microplate reader under excitation of 630 nm and emission of 670 nm.

2.16. In vivo anti-tumor evaluation in orthotopic U87MG-Luc glioma model

APS@(siRBBP4&TMZ), APS@(siScr&TMZ), APS@siRBBP4, PS@(siRBBP4&TMZ) (siRNA 1 mg/kg and TMZ 5 mg/kg), or PBS was administered via the tail vein into orthotopic U87MG-Luc glioma implanted nude mice at 10 days post-implantation. The nanomedicines were administered 5 times every two days. After the treatment termination, single mouse from every treatment group was sacrificed for further immunohistochemical assays. For luminescence distribution assays, pre-anesthetized mice were imaged with a Lumina IVIS-III system. During the treatment, the comparative luminescence intensity was calibrated to the initial intensity, and the individual body weights of the mice were normalized to the weights before injection. Within 47 days ($n = 6$), the Kaplan–Meier survival curve was calculated.

2.17. Immunohistochemistry

The excised tumor or organ tissue were fixed with formalin (10%, pH=7.0) and subsequently embedded in paraffin. The sections were then H&E stained to reveal histopathological alterations, and immunohistochemistry was used to identify RBBP4, MGMT, H2AX, Ki67, and Cas3. All images were acquired using digital microscopes. The signal intensities were determined as the average of five random areas of the same size and calculated using ImageJ software.

2.18. Statistical analysis

The presented are Mean ± SD. GraphPad Prism was used to process the survival longevity by the Kaplan-Meier technique. Log-rank test was used between treatment comparisons. For the rest of the studies, significance between treatments were calculated with one-way ANOVA test ($^{*}p < 0.05$, $^{**}p < 0.01$ and $^{***}p < 0.001$).

3. Results and discussion

3.1. Fabrication and characterization of polymersomal nanoparticles

We prepared the PEG-b-PFPMA-b-PGu (2-4.8–0.8 kDa) and Ang-PEG-b-PFPMA (3.4–4.7 kDa) polymers by a standard reversible addition-fragmentation chain transfer (RAFT) polymerization of FPMA and Gu monomers (for detailed synthesis information, please refer to Figs. S1, S2, S3). The synthesized polymers or their mixtures were dissolved in DMSO and dialyzed against water for nanoparticle formation. As shown in Fig. 2(a), the non-targeted polymers PEG-b-PFPMA-b-PGu and Ang-PEG-b-PGu/PEG-b-PFPMA-b-PGu polymer mixture solution (molar ration = 1:4) can self-assemble into nanoparticles with diameters of 86 nm (Angiopep-2 decorated polymersome, APS) and 78 nm (polymersome, PS), respectively. Strikingly, gel electrophoresis assays demonstrated that both APS and PS nanoparticles can completely and effectively load siRNAs within the aqueous lumen of polymersomes at a siRNA/polymer weight ratio of 1:10 (Fig. 2(b)). TEM showed that these siRNA-loaded nanoparticles had a distinctive spherical vesicular structure with siRNAs loaded in the aqueous interior (Fig. 2(c)), confirming the expected formation of the polymersomal nanostructure and successful siRNA loading. The formulated polymersome also loaded TMZ into its hydrophobic median layer with a loading efficiency of 28.4% at a theoretical loading content of 9% (Table S1). Notably, the TMZ- and siRNA-coloaded polymersomes showed slight size differences in comparison to the empty polymersomes, but their particle size remained less than 100 nm (Fig. S4). The effective loading of siRNA and TMZ indicated that the formulated polymersome is a suitable nanoparticle for TMZ and siRNA co-delivery, despite the divergent chemical nature of the compounds. Therefore, we explored its ability as a GBM chemo-RNAi synergistic therapy agent.

3.2. In vitro cell targeting and BBB traversing assays

Angiopep-2 is a peptide that not only facilitate the permeation of the BBB but can also target GBM cells through a well-known LRP-1 recognition, which is located on the BBB endothelial cells and overly expressed

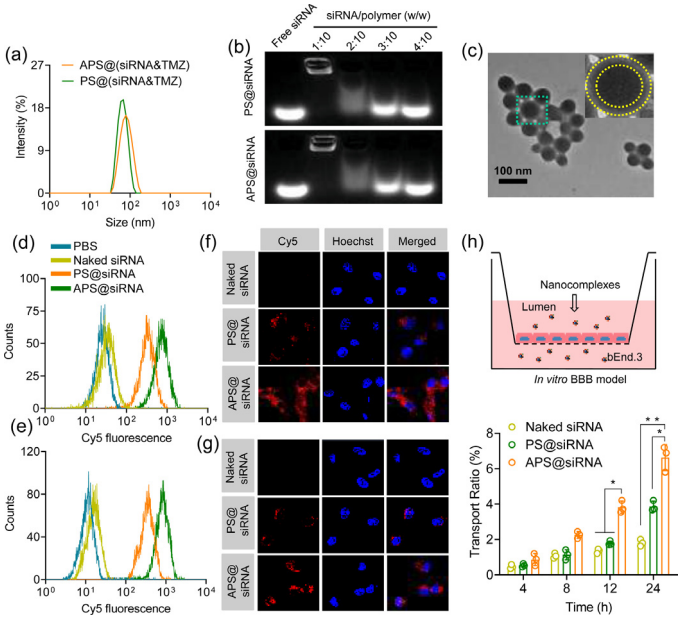

Fig. 2. Biophysical characterization of APS@siRNA and in vitro performance. (a) Size distribution of APS and PS. (b) Gel retardation of APS@siRNA and PS@siRNA with the siRNA/polymer weight ratio ranging from 1:10 to 4:10. (c) TEM images of APS@siRNA. Flow cytometry of (d) U87MG cells and (e) U251MG cells following 4 h incubation with PS@siRNA and APS@siRNA. CLSM micrographs of (f) U87MG cells and (g) U251MG cells incubated with PS@siRNA and APS@siRNA for 4 h. Cy5 labeled siRNA (red) and Hoechst-stained cell nuclei (blue) are shown in each panel, with overlays of the two images arranged from left to right. (h) At various time intervals, the cumulative transport ratios of PS@siRNA and APS@siRNA through an in vitro model of the BBB barrier. The data is presented as mean standard deviation ($n = 3$, $^{*}p < 0.05$, $^{**}p < 0.01$).

on the surface of human GBM cells [37]. This dual-targeting ability made Angiopep-2 as an ideal candidature to functionalize our nanomedicine for GBM-targeting therapeutics. In this study, both U87MG and U251MG cells were incubated with Cy5-labelled APS@siRNA for 4 h. Flow cytometry analysis (Fig. 2(d) and (e)) revealed that cellular uptake of APS@siRNA nanoparticles was superior versus the non-targeting counterpart PS@siRNA. CLSM images further confirmed this targeting ability; when U87MG and U251MG cells were incubated with APS@siRNA, we detected increased red fluorescence, demonstrating the increased APS@siRNA uptake by GBM cells (Fig. 2(f) and (g)). Notably, the high uptake of these polymeric nanoparticles resulted in negligible cytotoxicity (Fig. S5). Next, an in vitro BBB model was prepared by seeding a monolayer of bEnd.3 in a Transwell [44] to evaluate the BBB permeability of APS@(siRNA). Our findings demonstrated that Cy5-siRNA nanomedicines could cross the BBB in a time-dependent manner, with the accumulative transport ratio of APS@siRNA being substantially greater versus non-targeting PS@siRNA (Fig. 2(h)). This BBB and glioma cell dual-targeting ability endows these APS nanoparticles with great potential for use in GBM-targeting treatments in vivo.

3.3. In vitro synergistic anti-tumor effect

The insensitivity of glioma cells to TMZ can be attributed to the presence of methylguanine-DNA-methyltransferase (MGMT), which repairs TMZ-damaged DNA, thus reducing the impact of TMZ [7–9]. It was previously reported that RBBP4 is capable of modulating TMZ sensitivity by regulating MGMT [12]. Therefore, we predicted that the downregulation of RBBP4 would alter the sensitivity of TMZ. To this end, we co-loaded siRNAs that specifically target RBBP4 (siRBBP4) with TMZ into our polymersomes. Western blotting assays demonstrated that the siRBBP4-loaded nanoparticles (APS@(siRBBP4&TMZ) and

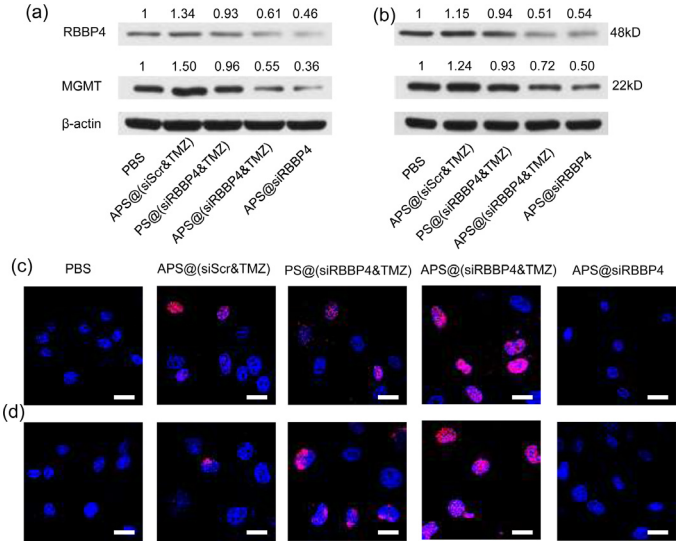

Fig. 3. In vitro synergistic effect of APS@(siRNA&TMZ). Expression levels of RBBP4 and MGMT protein in (a) U87MG cells and (b) U251MG cells after incubation with APS@(siRBBP4&TMZ). DNA damage assessment of (c) U87MG cells and (d) U251MG cells after incubation with APS@(siRBBP4&TMZ) using immunofluorescence of γH2AX. In all experiments, PBS, APS@(siScr&TMZ), PS@(siRBBP&TMZ), and APS@siRBBP4 were used as controls.

APS@siRBBP4) significantly downregulated the expression of RBBP4 as well as MGMT, in comparison to the control siRNA (scramble)-loaded counterpart APS@(siScr&TMZ), in both U87MG and U251MG cells (Fig. 3(a) and (b)). Moreover, the non-targeted PS@(siRBBP4&TMZ) displayed less RBBP4 and MGMT downregulation than its targeted counterpart, further confirming the targeting ability of Angiopep-2. Immunofluorescence results revealed that glioma cells treated with APS@(siRBBP4&TMZ) had significantly higher levels of γH2AX foci (a hallmark of DNA repair defects) compared with cells treated with APS@(siScr&TMZ) after 48 h incubation (Fig. 3(c) and (d)), suggesting that co-loading of TMZ and siRBBP4 leads to more severe DNA damage and confirming the synergistic therapeutic effect. Moreover, PS@(siRBBP4&TMZ) demonstrated low levels of γH2AX foci compared to APS@(siRBBP4&TMZ), further confirming the targeting effect of Angiopep-2. Taken together, these results suggest that our siRBBP4 and TMZ-co-loaded polymersomal delivery platform successfully exerted synergistic effects in vitro and, thus, has great potential for further in vivo antitumor applications.

3.4. In vivo pharmacokinetic and biodistribution

To perform an in vivo pharmacokinetic study, we injected the Balb/c mice through tail vein with the above-mentioned polymersomal nanoparticles encapsulating Cy5 labelled siRNA. As shown in Fig. 4(a), polymersomal nanoparticles with or without ligand modification had a similar prolonged elimination half-life ($t_{1/2,\beta}$= 42.6 and 46.3 min, respectively), which is considerably longer versus free siRNA ($t_{1/2,\beta}$ = 5.8 min). These results highlighting the prominence of nanoparticles for the stabilization and protection of siRNA in blood circulation, while validating that the Angiopep-2 peptide does not affect the pharmacokinetics of polymersomal nanoparticles.

For assessment of in vivo brain tumor-targeting ability of our polymersomal nanoparticles, U87MG-Luc orthotopic xenograft tumor models were prepared in BALB/c nude mice. The U87MG-Luc tumor-implanted nude mice were injected with Cy5-siRNA-encapsulated APS@siRNA and then imaged using a live mouse fluorescence imaging system (IVIS). The in vivo imaging study showed a strong Cy5 fluorescence intensity of APS@siRNA (Fig. 4(b)). Moreover, APS@siRNA

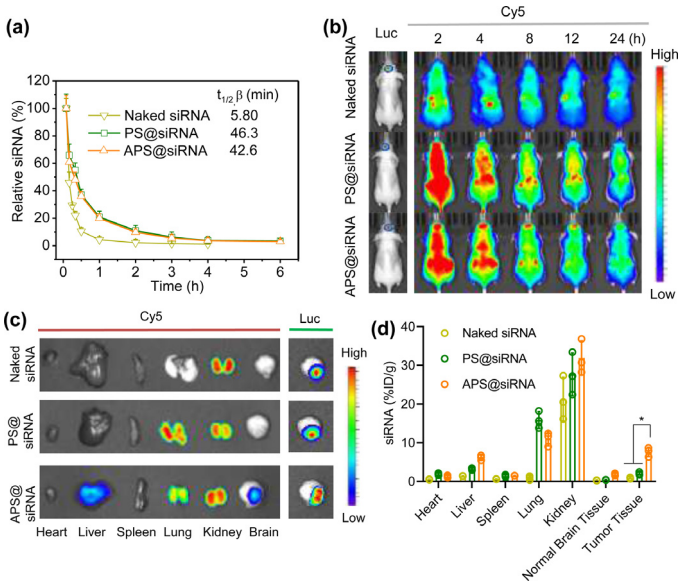

Fig. 4. Pharmacokinetics and biodistribution of APS@siRNA. (a) In vivo pharmacokinetics of APS@siRNA, PS@siRNA and free siRNA in mice. All siRNAs were labeled with Cy5. (b) Following injection of APS@siRNA, PS@siRNA, or free siRNA, fluorescence images of orthotopic U87MG-Luc human glioblastoma tumor-implanted nude mice at various time points. (c) Brain ex vivo fluorescence images after intravenous injections of APS@siRNA, PS@siRNA, and free siRNA. (d) The accumulation of siRNA in various organs 4 h post-administration of the APS@siRNA, PS@siRNA, or free siRNA was quantified. Fluorescence spectroscopy was used to determine the Cy5-siRNA levels, which were expressed as injected dose per gram of tissue (%ID/g). The mean and standard deviation are provided ($n = 3$, $^{*}p < 0.05$).

led to stronger accumulation in the brain tumor versus the non-ligand-decorated PS@siRNA (Fig. 4(b)), and we attribute this result to the superior BBB traversing ability and the GBM targeting ability of APS@siRNA. Ex vivo investigations further unveiled that mice treated with APS@siRNA had significantly higher Cy5 fluorescence in GBM than did those treated with PS@siRNA (Fig. 4(c)). Finally, biodistribution was measured by fluorometry, which revealed that APS@siRNA increased tumor accumulation by up to 7.6% of the administered dose per gram of tissue (% ID/g), which was 3.8- and 8.4-fold greater than PS@siRNA and siRNA controls, respectively (Fig. 4(d)).

3.5. *In vivo synergistic anti-tumor effect*

In orthotopically U87MG-luc glioma cells implanted mice, the synergistic anti-tumor activity of APS@(siRBBP4&TMZ) was examined. Ten days post-implantation, the U87MG-luc glioma tumorized nude mice were intravenously administered with APS@(siRBBP4&TMZ), PS@(siRBBP4&TMZ), APS@(siScr&TMZ), APS@(siRBBP4), and PBS every 2 days for 10 days. The findings indicate that APS@(siRBBP4&TMZ) can successfully inhibit glioma progression, as evidenced from the substantial decrease in Luc-bioluminescence (Fig. 5(a) and (b)) and a minor loss of body weight in the injected animals (Fig. 5(c)). By contrast, non-targeting (PS@(siRBBP4&TMZ)) and monotherapy counterparts (APS@(siScr&TMZ) and APS@siRBBP4) exhibited much weaker glioma growth inhibition than APS@(siRBBP4&TMZ) at the same siRNA and/or TMZ dosage (Fig. 5(a) and (b)), demonstrating the importance of active targeting and synergistic chemo-RNAi therapy. Moreover, these control groups displayed accelerated body weight loss (Fig. 5(c)) as a result of induced brain malfunction. In addition, we also observed that owing to these brain malfunctions, the glioma-bearing mice of control groups displayed symptoms of neurodegeneration (i.e tremor, problems with balance, or decreased move-

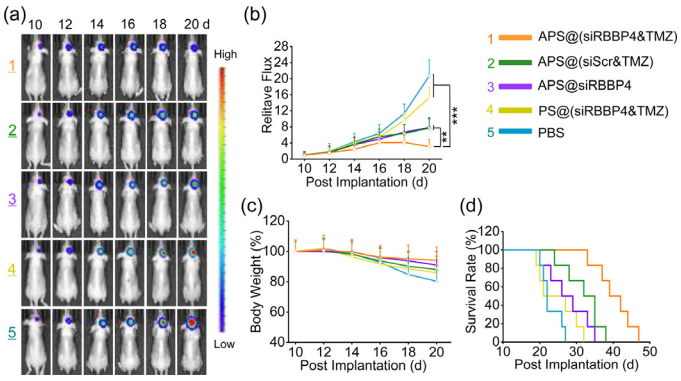

Fig. 5. In vivo synergistic anti-tumor effect of APS@(siRNA&TMZ). (a) Luminescence images of orthotopic U87MG-Luc human glioblastoma tumor-implanted nude mice treated with APS@(siRBBP4&TMZ). PBS, APS@(siScr&TMZ), PS@(siRBBP&TMZ) and APS@siRBBP4 were used as controls. (b) Luminescence levels of mice determined using the Lumina IVIS III system. Data are presented as mean ± SD, $^{*}p<0.05$, $^{**}p<0.005$, $^{***}p<0.001$. (c) Changes in mice body weight. (d) Mouse survival rates. Statistical analysis: APS@(siRBBP4&TMZ) vs APS@(siScr&TMZ), $^{*}p<0.05$; APS@(siRBBP4&TMZ) vs APS@siRBBP4 or PS@(siRBBP&TMZ), $^{**}p<0.01$; APS@(siRBBP4&TMZ) vs PBS, $^{***}p<0.001$ (Kaplan–Meier analysis, log-rank test).

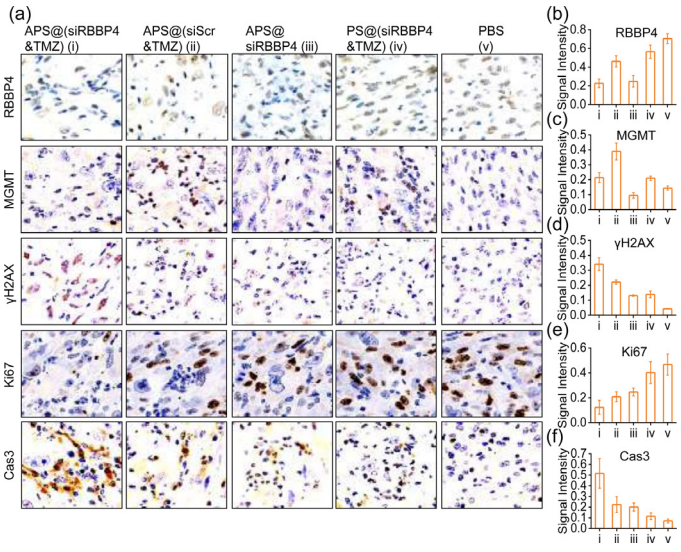

Fig. 6. Immunohistochemistry assays performed after treatment with APS@(siRNA&TMZ). Tumor slices were excised from nude mice bearing orthotopic U87MG-Luc human glioblastoma tumors following 10-day treatment with APS@(siRNA&TMZ) and were immunostained for RBBP4, MGMT, γH2AX, Ki67, and Cas3.

ments, data not shown). Survival figure showed APS@(siRBBP4&TMZ) group extended median survival time to 40 days, that was substantially longer compared to mice given PS@(siRBBP4&TMZ) (25 days), APS@(siScr&TMZ) (32 days), APS@siRBBP4 (28 days), or PBS (22 days) (Fig. 5(d)). These results highlighted the synergistic and targeted effects of APS@(siRBBP4&TMZ) for chemo-RNAi therapy. Tumor tissues from mice treated with these polymeric nanomedicines were further evaluated. As illustrated in Fig. 6, tumor tissues from mice injected with siRBBP4-based nanomedicine showed increased downregulation of RBBP4 and MGMT, while γH2AX foci evaluation revealed that APS@(siRBBP4&TMZ) exhibited the most severe DNA damaging effect. Furthermore, the APS@(siRBBP4&TMZ)-treated group displayed the maximum level of apoptosis in tumor cells (Cas3), but had the lowest level of tumor cell proliferation (Ki67).

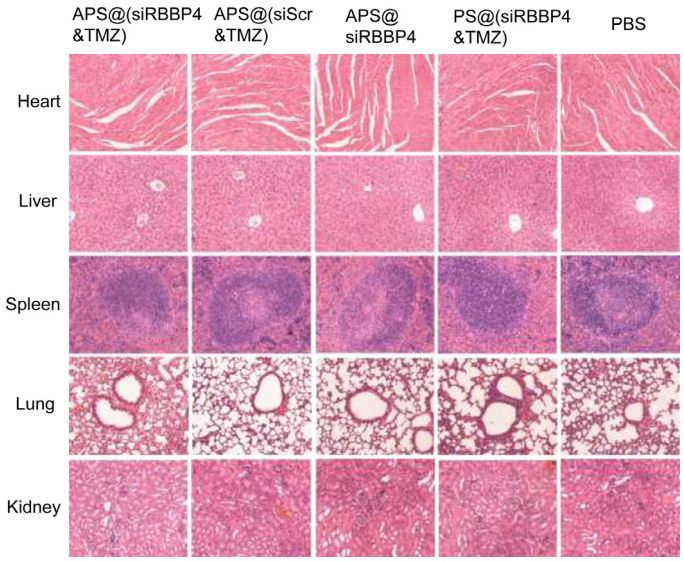

Fig. 7. Biocompatibility assay of APS@(siRNA&TMZ). H&E-stained slices of the heart, liver, spleen, lung and kidney were examined histologically after 10 days of treatment, excised from the tumor-implanted mice.

3.6. Biocompatibility assay

H&E staining was performed for heart, liver, spleen, lung, and kidney at the termination the tumor inhibition assay. The results showed that no organ damage was observed in all treatment groups (Fig. 7), demonstrated an extraordinary biocompatibility of our polymersomal nanomedicines. Additionally, blood chemistry analyses (Fig. S6) demonstrated mice treated with APS@(siRBBP4&TMZ) or PBS had identical levels of blood plasma aspartate aminotransferase (AST), alanine aminotransferase (ALT), alkaline phosphatase (ALP), plasma urea (BUN), creatinine (CR), and uric acid (UA) similar counts of blood platelets (PLT), red blood cells (RBCs), and white blood cells (WBCs). This further verify the biocompatibility of this chemo-RNAi nanomedicine. These results suggest that APS@(siRBBP4&TMZ) provides safe and greatly effectual antitumor activity in an orthotopic glioma mouse model.

4. Conclusion

In summary, we developed a brain-targeted siRNA- and TMZ-coloaded polymersomal delivery system (APS@(siRNA&TMZ)). APS@(siRNA&TMZ) not only enhanced the circulation time of encapsulated drugs in the blood, but also improved BBB crossing and GBM targeting abilities. Moreover, when APS@(siRNA&TMZ) was actively taken up by glioma cells, the delivered siRNA increased the TMZ-sensitivity of glioma cells by knocking down RBBP4, thus regulating TMZ-related DNA-damage repair through MGMT. Our results on combined chemo-RNAi GBM therapy showed that this polymersomal nanomedicine has powerful synergistic anti-tumor effects and could suppress the malignancy to significantly improve survival times in mice. These findings suggest that this TMZ/siRNA codelivery system is a robust and potent nanoplatform for targeted anti-GBM chemo-RNAi therapy.

Declaration of Competing Interest

The authors declare that they have no conflict of interest.

Acknowledgment

This research was funded by China's National Key Technologies R&D Programs (2018YFA0209800), National Natural Science Foundation of China (NSFC 52073079, 31800841, 32071388, and U1804139), Key Research Program in Colleges and Universities of Henan Province (19zx006), Program of Technology Innovation Team in Colleges and Universities of Henan Province (21IRTSTHN028), and NHMRC Investigator Grant.

Supplementary materials

Supplementary material associated with this article can be found, in the online version, at doi:10.1016/j.chphma.2022.01.001.

References

[1] B.M. Alexander, T.F. Cloughesy, Adult glioblastoma, J. Clin. Oncol. 35 (2017) 2402–2409.
[2] K. Aldape, G. Zadeh, S. Mansouri, et al., Glioblastoma: pathology, molecular mechanisms and markers, Acta Neuropathol. 129 (2015) 829–848.
[3] P.D. Delgado-Lopez, E.M. Corrales-Garcia, Survival in glioblastoma: a review on the impact of treatment modalities, Clin. Transl. Oncol. 18 (2016) 1062–1071.
[4] C. Adamson, O.O. Kanu, A.I. Mehta, et al., Glioblastoma multiforme: a review of where we have been and where we are going, Expert Opin. Investig. Drug 18 (2009) 1061–1083.
[5] J. Zhang, M.F. Stevens, T.D. Bradshaw, Temozolomide: mechanisms of action, repair and resistance, Curr. Mol. Pharmacol. 5 (2012) 102–114.
[6] S.Y. Lee, Temozolomide resistance in glioblastoma multiforme, Genes Dis. 3 (2016) 198–210.
[7] F. Drablos, E. Feyzi, P.A. Aas, et al., Alkylation damage in DNA and RNA–repair mechanisms and medical significance, DNA Repair (Amst.) 3 (2004) 1389–1407.
[8] M.E. Hegi, L. Liu, J.G. Herman, et al., Correlation of O6-methylguanine methyltransferase (MGMT) promoter methylation with clinical outcomes in glioblastoma and clinical strategies to modulate MGMT activity, J. Clin. Oncol. 26 (2008) 4189–4199.
[9] G.J. Kitange, B.L. Carlson, M.A. Schroeder, et al., Induction of MGMT expression is associated with temozolomide resistance in glioblastoma xenografts, Neuro-Oncology 11 (2009) 281–291.
[10] R. Stupp, M.E. Hegi, W.P. Mason, et al., Effects of radiotherapy with concomitant and adjuvant temozolomide versus radiotherapy alone on survival in glioblastoma in a randomised phase III study: 5-year analysis of the EORTC-NCIC trial, Lancet Oncol. 10 (2009) 459–466.
[11] A. Murat, E. Migliavacca, T. Gorlia, et al., Stem cell-related "self-renewal" signature and high epidermal growth factor receptor expression associated with resistance to concomitant chemoradiotherapy in glioblastoma, J. Clin. Oncol. 26 (2008) 3015–3024.
[12] G.J. Kitange, A.C. Mladek, M.A. Schroeder, et al., Retinoblastoma binding protein 4 modulates temozolomide sensitivity in glioblastoma by regulating DNA repair proteins, Cell Rep. 14 (2016) 2587–2598.
[13] M. Zheng, W. Tao, Y. Zou, et al., Nanotechnology-based strategies for siRNA brain delivery for disease therapy, Trends Biotechnol. 36 (2018) 562–575.
[14] R.L. Setten, J.J. Rossi, S.P. Han, The current state and future directions of RNAi-based therapeutics, Nat. Rev. Drug Discov. 18 (2019) 421–446.
[15] M.L. Bobbin, J.J. Rossi, RNA interference (RNAi)-based therapeutics: delivering on the promise? Annu. Rev. Pharmacol. Toxicol. 56 (2016) 103–122.
[16] M. Creixell, N.A. Peppas, Co-delivery of siRNA and therapeutic agents using nanocarriers to overcome cancer resistance, Nano Today 7 (2012) 367–379.
[17] M. Zheng, T. Jiang, W. Yang, et al., The siRNAsome: a cation-free and versatile nanostructure for siRNA and drug co-delivery, Angew. Chem. Int. Ed. 58 (2019) 4938–4942.
[18] Y. Lu, L. Liu, Y. Wang, et al., siRNA delivered by EGFR-specific scFv sensitizes EGFR-TKI-resistant human lung cancer cells, Biomaterials 76 (2016) 196–207.
[19] Y.H. Yu, E. Kim, D.E. Park, et al., Cationic solid lipid nanoparticles for co-delivery of paclitaxel and siRNA, Eur. J. Pharm. Biopharm. 80 (2012) 268–273.
[20] R. Pandit, L. Chen, J. Gotz, The blood-brain barrier: Physiology and strategies for drug delivery, Adv. Drug. Deliv. Rev. (2020) 165–166 1-14.
[21] J. Xie, Z. Shen, Y. Anraku, et al., Nanomaterial-based blood-brain-barrier (BBB) crossing strategies, Biomaterials 224 (2019) 119491.
[22] X. Dong, Current strategies for brain drug delivery, Theranostics 8 (2018) 1481–1493.
[23] T. Jiang, Y.H. Qiao, W.M. Ruan, et al., Cation-free siRNA micelles as effective drug delivery platform and potent RNAi nanomedicines for glioblastoma therapy, Adv. Mater. 33 (2021) 2104779.
[24] Y. Jiang, J. Zhang, F.H. Meng, et al., Apolipoprotein E peptide-directed chimeric polymersomes mediate an ultrahigh-efficiency targeted protein therapy for glioblastoma, ACS Nano 12 (2018) 11070–11079.
[25] S.A. Elkassih, P. Kos, H. Xiong, et al., Degradable redox-responsive disulfide-based nanogel drug carriers via dithiol oxidation polymerization, Biomater. Sci. 7 (2019) 607–617.
[26] J. Liu, C. Chen, T. Wei, et al., Dendrimeric nanosystem consistently circumvents heterogeneous drug response and resistance in pancreatic cancer, Exploration 1 (2021) 21–34.
[27] S. Guo, K. Li, B. Hu, et al., Membrane-destabilizing ionizable lipid empowered imaging-guided siRNA delivery and cancer treatment, Exploration 1 (2021) 35–49.

[28] H. Huang, C. Dong, M. Chang, et al., Mitochondria-specific nanocatalysts for chemotherapy-augmented sequential chemoreactive tumor therapy, Exploration 1 (2021) 50–60.
[29] J. Jacob, J.T. Haponiuk, S. Thomas, et al., Biopolymer based nanomaterials in drug delivery systems: a review, Mater. Today Chem. 9 (2018) 43–55.
[30] F.H. Meng, Z.Y. Zhong, Polymersomes spanning from nano- to microscales: advanced vehicles for controlled drug delivery and robust vesicles for virus and cell mimicking, J. Phys. Chem. Lett. 2 (2011) 1533–1539.
[31] L. Zhao, N. Li, K. Wang, et al., A review of polypeptide-based polymersomes, Biomaterials 35 (2014) 1284–1301.
[32] V. Balasubramanian, B. Herranz-Blanco, P.V. Almeida, et al., Multifaceted polymersome platforms: Spanning from self-assembly to drug delivery and protocells, Prog. Polym. Sci. 60 (2016) 51–85.
[33] J. Zou, C. Jin, R. Wang, et al., Fluorinated DNA micelles: Synthesis and properties, Anal. Chem. 90 (2018) 6843–6850.
[34] L.H. Wang, D.C. Wu, H.X. Xu, et al., High DNA-binding affinity and gene-transfection efficacy of bioreducible cationic nanomicelles with a fluorinated core, Angew. Chem. Int. Ed. 55 (2016) 755–759.
[35] Z. Zhang, W. Shen, J. Ling, et al., The fluorination effect of fluoroamphiphiles in cytosolic protein delivery, Nat. Commun. 9 (2018) 1377.
[36] Y. Zhao, W. Wang, S. Guo, et al., PolyMetformin combines carrier and anticancer activities for in vivo siRNA delivery, Nat. Commun. 7 (2016) 11822.
[37] P.K. Hashim, K. Okuro, S. Sasaki, et al., Reductively cleavable nanocaplets for siRNA delivery by template-assisted oxidative polymerization, J. Am. Chem. Soc. 137 (2015) 15608–15611.
[38] Y. Zhou, F. Zhu, Y. Liu, et al., Blood-brain barrier-penetrating siRNA nanomedicine for Alzheimer's disease therapy, Sci. Adv. 6 (2020) eabc7031.
[39] M. Zheng, Y. Liu, Y. Wang, et al., ROS-responsive polymeric siRNA nanomedicine stabilized by triple interactions for the robust glioblastoma combinational RNAi therapy, Adv. Mater. 31 (2019) e1903277.
[40] Y. Zou, Y. Liu, Z. Yang, et al., Effective and targeted human orthotopic glioblastoma xenograft therapy via a multifunctional biomimetic nanomedicine, Adv. Mater. 30 (2018) e1803717.
[41] Y.J. Liu, Y. Zou, C. Feng, et al., Charge conversional biomimetic nanocomplexes as a multifunctional platform for boosting orthotopic glioblastoma RNAi therapy, Nano Lett. 20 (2020) 1637–1646.
[42] Y. Zou, X. Sun, Y. Wang, et al., Single siRNA nanocapsules for effective siRNA brain delivery and glioblastoma treatment, Adv. Mater. 32 (2020) e2000416.
[43] S. Huang, J. Li, L. Han, et al., Dual targeting effect of Angiopep-2-modified, DNA-loaded nanoparticles for glioma, Biomaterials 32 (2011) 6832–6838.
[44] Y. Shi, Y. Jiang, J. Cao, et al., Boosting RNAi therapy for orthotopic glioblastoma with nontoxic brain-targeting chimaeric polymersomes, J. Control Release 292 (2018) 163–171.